ELSEVIER

Lithos 55 (2001) 101–114

LITHOS

www.elsevier.nl/locate/lithos

Thermodynamic modelling of C–O–H fluids

Jan-Marten Huizenga *

Department of Geology, Rand Afrikaans University, PO Box 524, Auckland Park 2006, Johannesburg, South Africa

Received 7 March 2000; accepted 25 April 2000

Abstract

H_2O, CO_2, CH_4, CO, H_2 and O_2 are the most important species in crustal fluids. The composition of these C–O–H fluids can be calculated if the pressure, temperature, carbon activity, and either the oxygen fugacity or the atomic H/O ratio of the fluid is known. The calculation methods are discussed and calculation results are illustrated with isobaric T–X_i, P–T, and isobaric–isothermal ternary C–O–H diagrams. Fluid inclusion compositions, in particular, the $X_{CO_2}/(X_{CO_2}+X_{CH_4})$ ratio, can be used for C–O–H model calculations. However, care should be taken about possible post-entrapment changes, which may have modified the chemical composition of the fluid inclusion.

Keywords: Fluid speciation; Thermodynamic modelling; C–O–H system; Fluid inclusions

1. Introduction

Many metamorphic and igneous fluids can be described by three components: carbon, oxygen and hydrogen (the C–O–H system). The principal fluid species of geological interest in this system are: H_2O, CO_2, CH_4, CO, H_2 and O_2 (French, 1966; Ohmoto and Kerrick, 1977; Holloway, 1987). French (1966) and Ohmoto and Kerrick (1977) have demonstrated that this system can be used to calculate the composition of crustal fluids as a function of P_{fluid}, T, and either the oxygen fugacity ($f_{O_2}^{fluid}$) or the H/O atomic ratio of the fluid. C–O–H model calculations have been used by many authors for a variety of geological subjects, such as fluid equilibria at low-grade metamorphism (e.g., Holloway, 1984), granulite genesis (e.g., Glassley, 1982; Lamb and Valley, 1985; Skippen and Marshall, 1991) and devolatilisation reactions in graphitic rocks (Connolly and Cesare, 1993; Connolly, 1995).

This paper reviews the method for C–O–H model calculations. The results are shown in different diagrams and illustrate the influence of different variables (i.e. P_{fluid}, T, $f_{O_2}^{fluid}$, atomic H/O ratio) on the fluid speciation. The applications and limitations of C–O–H model calculations to fluid inclusion studies will also be discussed.

2. Calculation method

2.1. Basic principles

The calculation method used follows the procedure given by French (1966) and is based on the

* Fax: +27-11-489-2309.
E-mail address: jmh@na.rau.ac.za (J.-M. Huizenga).

0024-4937/01/$ - see front matter
PII: S0024-4937(00)00040-2

equilibrium constant-mass balance technique (French, 1966; Eugster and Skippen, 1967; Ohmoto and Kerrick, 1977, Holloway, 1987; Spear, 1993). The calculations are valid for a homogeneous, intergranular fluid, which does not react with solid phases, except for graphite, in the rock (e.g., Miyashiro, 1994). The blocking temperature of the fluid–graphite equilibrium is estimated to be ~400°C (Ramboz et al., 1985). Therefore, C–O–H model calculations for carbon-saturated fluids cannot be done at temperatures below 400°C.

The calculations have been described in detail by, e.g., French (1966), Ohmoto and Kerrick (1977), Holloway (1987), Labotka (1991) and Skippen and Marshall (1991). At a fixed P_{fluid} and T, the system has seven unknowns: the fluid speciation (X_{H_2O}, X_{CO_2}, X_{CH_4}, X_{H_2} and X_{CO}), $f_{O_2}^{\text{fluid}}$, and the carbon activity (a_{carbon}). Four independent chemical equilibria can be written (French, 1966; Ohmoto and Kerrick, 1977):

$$CO + \tfrac{1}{2}O_2 = CO_2 \quad (1)$$

$$H_2 + \tfrac{1}{2}O_2 = H_2O \quad (2)$$

$$CH_4 + 2O_2 = CO_2 + 2H_2O \quad (3)$$

$$C + O_2 = CO_2 \quad (4)$$

with the following equilibrium constants (K_{1-4}):

$$K_1 = \frac{f_{CO_2}}{f_{CO}\left(f_{O_2}\right)^{1/2}} \quad (5)$$

$$K_2 = \frac{f_{H_2O}}{f_{H_2}\left(f_{O_2}\right)^{1/2}} \quad (6)$$

$$K_3 = \frac{f_{CO_2}\left(f_{H_2O}\right)^2}{f_{CH_4}\left(f_{O_2}\right)^2} \quad (7)$$

$$K_4 = \frac{f_{CO_2}}{a_{\text{carbon}} f_{O_2}} \quad (8)$$

a_{carbon} in Eq. (8) is unity if graphite is present, whereas it has a value between 0 and 1 if the fluid is undersaturated in carbon. P_{fluid} can be related to the hydrostatic pressure gradient or the lithostatic pressure gradient. The mass balance constraint yields (ignoring X_{O_2}):

$$X_{H_2O} + X_{CO_2} + X_{CH_4} + X_{CO} + X_{H_2} = 1 \quad (9)$$

The relation between the fugacity and the mole fraction of species i is given by (e.g., Ferry and Baumgartner, 1987; Anderson and Crerar, 1993; Spear, 1993):

$$f_i = X_i \gamma_i P_{\text{fluid}} \quad (10)$$

where γ_i denotes the fugacity coefficient of species i. Eq. (10) is based on the assumption of ideal mixing, which is a reasonable approximation for supercritical, (i.e. $T > 400$°C) homogeneous fluids (e.g., Labotka, 1991). Eq. (10) can be substituted into Eqs. (5)–(8) in order to express the equilibrium constant as a function of the mole fractions of the principal fluid species.

For a carbon-saturated C–O–H fluid, one additional constraint is needed to calculate the fugacities of all fluid species. For example, $f_{O_2}^{\text{fluid}}$ can be buffered by a mineral assemblage and the remaining five fugacities can then be calculated (e.g., French, 1966; Ohmoto and Kerrick, 1977). Alternatively, one can also fix the atomic H/O ratio (French, 1966; Ohmoto and Kerrick, 1977; Labotka, 1991; Connolly and Cesare, 1993; Connolly, 1995) or the mole fraction of carbon relative to hydrogen in the fluid phase (Frost, 1979), and calculate all six fugacities. Although these alternatives are used by many authors (e.g., French, 1966; Ohmoto and Kerrick, 1977; Frost, 1979; Holloway, 1984; Labotka, 1991; Connolly and Cesare, 1993; Connolly, 1995), it must be emphasized that these are just possibilities. It is, for example, also possible to fix $f_{O_2}^{\text{fluid}}$ and f_{H_2} in order to calculate the remaining four fugacities and P_{fluid} (Skippen and Marshall, 1991). Which additional constraint to use depends on the particular problem one wants to solve and the geological data that is available. In this paper, the two most commonly used methods will be discussed in more detail.

2.2. Externally buffered oxygen fugacity

$f_{O_2}^{\text{fluid}}$ can be buffered by a mineral assemblage, such as Quartz–Fayalite–Magnetite (QFM), $f_{O_2}^{\text{fluid}} = f_{O_2}^{\text{QFM}}$, according to the equilibrium:

$$3Fe_2SiO_4 + O_2 = 2Fe_3O_4 + 3SiO_2 \quad (11)$$

where $f_{O_2}^{QFM}$ can be calculated from the Gibbs energy of the reaction ($\Delta_r G_{QFM}^{O}$) assuming unit activities for olivine and magnetite (e.g., Anderson and Crerar, 1993):

$$\Delta_r G_{QFM}^{O} = RT \ln f_{O_2}^{QFM} \quad (12)$$

where R denotes the gas constant (8.314 J mol^{-1} K^{-1}). The calculations will then proceed as follows (e.g., Ohmoto and Kerrick, 1977). X_{CO_2} can be calculated from Eq. (8):

$$X_{CO_2} = \left[\frac{K_4 f_{O_2}^{QFM}}{\gamma_{CO_2} P_{fluid}} \right]_{C_1} \quad (13)$$

where the parameters within the square bracket (labeled with C_1) are constant at a fixed P_{fluid} and T. Eq. (5) will give for X_{CO}:

$$X_{CO} = \left[\frac{\gamma_{CO_2}}{K_1 \gamma_{CO} \left(f_{O_2}^{QFM} \right)^{1/2}} \right]_{C_2} X_{CO_2} \quad (14)$$

X_{H_2} and X_{CH_4} explicit equations can be derived from Eqs. (6) and (7), respectively:

$$X_{H_2} = \left[\frac{\gamma_{H_2O}}{K_2 \gamma_{H_2} \left(f_{O_2}^{QFM} \right)^{1/2}} \right]_{C_3} X_{H_2O} \quad (15)$$

$$X_{CH_4} = \left[\frac{\gamma_{CO_2} \left(\gamma_{H_2O} \right)^2 \left(P_{fluid} \right)^2}{K_3 \gamma_{CH_4} \left(f_{O_2}^{QFM} \right)^2} \right]_{C_4} X_{CO_2} \left(X_{H_2O} \right)^2 \quad (16)$$

Substitution of Eqs. (13)–(16) into Eq. (9) will give a quadratic expression for:

$$C_1 C_4 \left(X_{H_2O} \right)^2 + C_3 X_{H_2O} + \left(C_1 + C_1 C_2 - 1 \right) = 0 \quad (17)$$

where C_1, C_2, C_3 and C_4 are the expressions indicated in Eqs. (13)–(16), respectively. The positive root of Eq. (17) will give the correct answer for X_{H_2O}. Subsequently, the molar volume of the fluid can be calculated using the fluid composition, P_{fluid} and T from any equation of state that is appropriate for fluid mixtures, such as the Redlich–Kwong equation of state (Redlich and Kwong, 1949), modified by Holloway (1981).

2.3. Fixed atomic H / O ratio

The carbon content in a C–O–H fluid in equilibrium with graphite depends on P_{fluid} and T in order to maintain carbon saturation (Connolly, 1995). Fluid speciation at a constant atomic H/O ratio has the advantage that it is independent of pressure and temperature (Connolly, 1995). Using this approach, all fugacities (including $f_{O_2}^{fluid}$), can be solved from Eqs. (9), (13)–(16), and (18), which fixes the atomic H/O ratio or X_O, which is defined as (Labotka, 1991; Connolly, 1995):

$$X_O \equiv \frac{n_O}{n_O + n_H} \quad (18)$$

where n_O and n_H are the number of moles of oxygen and hydrogen in the fluid phase, respectively, i.e.

$$n_O = X_{H_2O} + 2 X_{CO_2} + X_{CO} + 2 X_{O_2} \quad (19)$$

$$n_H = 2 X_{H_2O} + 4 X_{CH_4} + 2 X_{H_2} \quad (20)$$

A description of the calculation procedure for C–O–H fluid speciation as a function of X_O is given by Connolly (1995).

2.4. Equilibrium constants

The equilibrium constants K_1–K_4 can be calculated using different thermodynamic data sets. Ohmoto and Kerrick (1977) give P_{fluid}–T equations for the equilibrium constants using thermodynamic data from Holland (1965) and Huebner (1971) and are easy to use in model calculations. The equilibrium constant can also be derived from the Gibbs energy of the reaction (e.g., Anderson and Crerar, 1993):

$$\Delta_r G^{O} = -RT \ln K \quad (21)$$

where $\Delta_r G^O$ can be calculated from the formation enthalpy, entropy and isobaric heat capacity of the fluid species given by, e.g., Chase et al. (1985), Shi and Saxena (1992) or Holland and Powell (1998). Thermodynamic properties of graphite can be taken from, e.g., Holland and Powell (1998). $\log_{10} K_{1-4}$ values calculated from different data sets (Ohmoto and Kerrick, 1977; Shi and Saxena, 1992; Holland and Powell, 1998) do not show significant differences (i.e. less than 5‰).

2.5. Fugacity coefficients

Eq. (10) shows that the fugacity coefficient for a pure fluid ($X_i = 1$) can be expressed as:

$$\gamma_i = \frac{f_i}{P_{fluid}} \tag{22}$$

where f_i can be calculated from the following expression (e.g., Chatterjee, 1991; Anderson and Crerar, 1993):

$$\int_1^{P_{fluid}} V(P_{fluid}, T)\,dP = RT \ln f(P_{fluid}, T) \tag{23}$$

where V is the molar volume of the fluid phase. This equation can be rewritten in many different ways, depending on the form in which the equation of state is written. For example, consider a virial type equation of state (e.g., Ferry and Baumgartner, 1987; Saxena and Fei, 1987a; Chatterjee, 1991):

$$Z \equiv \frac{P_{fluid} V}{RT} = 1 + BP_{fluid} + CP_{fluid}^2 DP_{fluid}^3 \tag{24}$$

where Z is the compressibility factor, and B, C, and D are functions of the temperature. For this equation of state, the fugacity can be expressed as follows:

$$\ln f(P_{fluid}, T) = \int_1^{P_{fluid}} \frac{Z}{P_{fluid}}\,dP \tag{25}$$

assuming that the standard state fugacity is 1 bar. The expression for the fugacity coefficient will then become (Shi and Saxena, 1992):

$$\ln \gamma(P_{fluid}, T) = \int_1^{P_{fluid}} \frac{Z}{P_{fluid}}\,dP - \ln P_{fluid} \tag{26}$$

Detailed reviews of different equations of state and calculation of fugacities and fugacity coefficients are given by, e.g., Ferry and Baumgartner (1987), Chatterjee (1991), and Labotka (1991).

Ohmoto and Kerrick (1977) used an ideal mixing model and calculated the fugacity coefficients of the fluid species from thermodynamic data given by Burnham et al. (1969), Burnham and Wall (unpublished data), Shaw and Wones (1964), and Ryzhenko and Volkov (1971). For non-ideal mixing, the fugacity coefficient is a function of P_{fluid}, T, and fluid composition (e.g., Flowers and Helgeson, 1983). Non-ideal mixing fugacity coefficients can be calculated from the Modified Redlich Kwong equation of state (Holloway, 1977, 1981; Flowers and Helgeson, 1983) and should be used at temperatures close to the immiscibility region of the aqueous–carbonic system (Connolly and Cesare, 1993). At temperatures greater than 400°C, fluid mixing properties have small deviations from ideality (Labotka, 1991; Sterner and Bodnar, 1991).

2.6. Computer programs

Several computer programs are available to calculate the C–O–H fluid speciation. 'GEOFLUID' is a program written by Larsen (1993) and uses the same thermodynamic data set as given by Ohmoto and Kerrick (1977) for calculating equilibrium constants. Ideal mixing fugacity coefficients are calculated from Burnham et al. (1969), Burnham and Wall (unpublished data), Shaw and Wones (1964), Ryzhenko and Volkov (1971), Saxena and Fei (1987a), and Jacobs and Kerrick (1981).

The PERPLEX program (Connolly, 1990, 1995) includes the fluid speciation program 'COHSRK' for the C–O–H and the C–O–H–S system, using (amongst others) X_O or $f_{O_2}^{fluid}$ as input parameters. The program gives many options to choose from. Detailed information can be derived from the web site: http://eurasia.ethz.ch/~jamie/perplex.html.

Belonoshko et al. (1992) have written the program 'SUPERFLUID', which calculates the Gibbs energy and fugacity coefficients for fluid species within the C–O–H–N–S–Ar system. The program is based on thermodynamic properties and equations

of state given by Saul and Wagner (1989), Jacobs and Kerrick (1981), Belonoshko and Saxena (1991a,b, 1992), and Shi and Saxena (1992).

2.7. Limitations and uncertainties of C–O–H model calculations

A number of factors limits the use of C–O–H model calculations. First, the presence of electrolytes, such as NaCl, KCl, $CaCl_2$, etc., will influence the fugacity coefficient of H_2O (e.g., Aranovich and Newton, 1996) and it will also raise the solvus temperature of the aqueous–carbonic fluid system (e.g., Bowers and Helgeson, 1983), implying that one should rather apply a non-ideal mixing model (e.g., Connolly and Cesare, 1993) using a Modified Redlich–Kwong type equation of state (Holloway, 1977, 1981) that includes NaCl. Bakker (1999) has recently published an equation of state for the H_2O–CO_2–CH_4–N_2–NaCl system, but unfortunately, this equation of state is not valid for fluids close to fluid–fluid unmixing conditions (Bakker, 1999).

Second, the fluid phase may not be in equilibrium with graphite (Connolly and Cesare, 1993), or graphite might have some degree of disorder, which will change its thermodynamic properties and, therefore, the equilibrium constant K_4 (Ziegenbein and Johannes, 1980). The degree of disorder of graphite can be identified from Raman spectra (e.g., Burke, 1994; Wopenka and Pasteris, 1993).

Third, one should be careful with the interpretation of the calculation results as these might show significant differences when different equations of state are used for the calculation of fugacity coefficients. Furthermore, when $f_{O_2}^{fluid}$ is externally buffered by a mineral assemblage such as QFM, different thermodynamic datasets may give different results for $f_{O_2}^{QFM}$. This will lead to different fluid compositions as the C–O–H system is sensitive for small differences in $f_{O_2}^{fluid}$.

3. Calculation results

In this study, the equilibrium constants K_{1-4} and $f_{O_2}^{QFM}$ were calculated from the thermodynamic data set after Holland and Powell (1998). Fugacity coefficients were calculated from the virial equations of state after Saxena and Fei (1987a,b), assuming ideal mixing. The calculations are valid for P_{fluid} and T greater than 1 kbar and 400°C, respectively. The results are illustrated with P–T, isobaric X_i–T, and isobaric–isothermal ternary C–O–H diagrams.

3.1. Externally buffered oxygen fugacity

Fig. 1 shows the temperature dependence of the fluid at a fixed P_{fluid} of 3 kbar and $f_{O_2}^{fluid}$ buffered by QFM and one $\log_{10}$ unit below QFM. At low temperatures, the fluid is dominated by H_2O–CH_4, where X_{CH_4} depends on $f_{O_2}^{fluid}$, i.e. at the same temperature, X_{CH_4} is greater if $f_{O_2}^{fluid}$ is one $\log_{10}$ unit below $f_{O_2}^{QFM}$ (Fig. 1A,B). With increasing temperature (i.e. increasing $f_{O_2}^{fluid}$; see Fig. 1), X_{CH_4} decreases at the expense of CO_2 and H_2O. X_{H_2O} will reach its maximum value at a certain temperature and then decrease with increasing temperature until the maximum stability temperature of graphite is reached and the fluid becomes pure CO_2, i.e. all graphite is oxidised to CO_2. For a QFM buffered fluid, the maximum stability temperature of graphite is ~ 570°C at 3 kbar and $\log_{10} f_{O_2}^{fluid} = \log_{10} f_{O_2}^{QFM} = \sim -20.8$ (Figs. 1A and 2). Carbon undersaturated fluids (Fig. 1C, $a_{carbon} = 0.1$) do not contain significant amounts of CH_4 and the fluid is dominated by H_2O. CO_2 is only present at relative high temperatures.

Fig. 3 shows the fluid speciation in P–T diagrams, where $f_{O_2}^{fluid} = f_{O_2}^{QFM}$ and $f_{O_2}^{fluid} = f_{O_2}^{QFM\text{-}1}$. The diagrams illustrate, similar to Fig. 1, an increase of X_{CO_2} with increasing temperature at the expense of CH_4 and H_2O. It also demonstrates the pressure sensitivity of X_{H_2O} up to a certain temperature (i.e. ~ 500°C for $f_{O_2}^{fluid} = f_{O_2}^{QFM}$; see Fig. 3A). Above that temperature, X_{H_2O} mainly depends on the temperature. The stability field of graphite is extended to greater temperatures when more reducing buffers (e.g., $f_{O_2}^{fluid} = f_{O_2}^{QFM\text{-}1}$) are used (Figs. 1B and 3B). A carbon undersaturated fluid (Figs. 1C and 3C) is dominated by H_2O over a large temperature range. CH_4 does not occur in significant amounts and CO_2 will only become dominantly present at high temperatures.

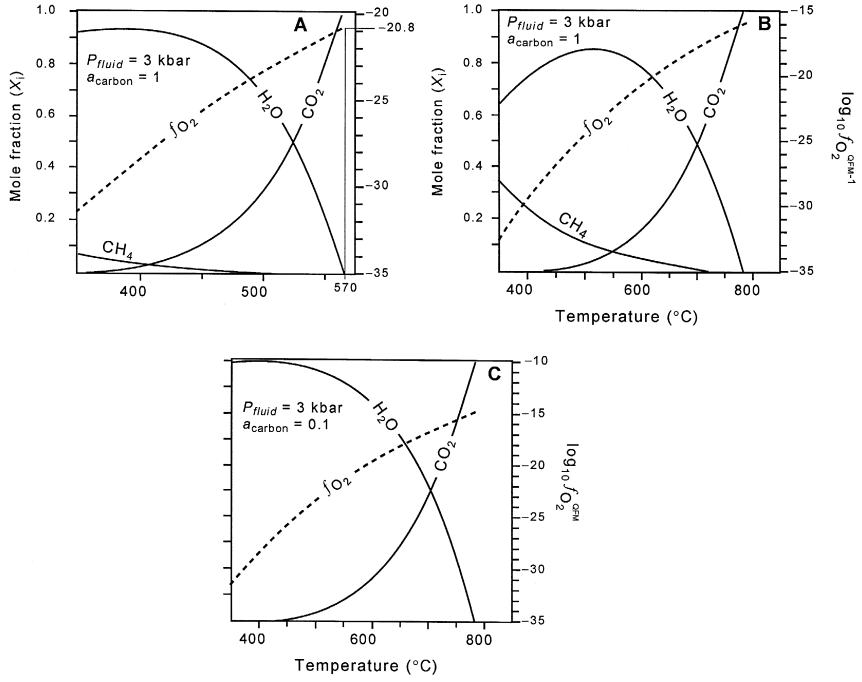

Fig. 1. Compositional variation of a C–O–H fluid as a function of temperature ($P_{\text{fluid}} = 3$ kbar). (A) Carbon saturated fluid ($a_{\text{carbon}} = 1$), $f_{O_2}^{\text{fluid}} = f_{O_2}^{\text{QFM}}$. Graphite becomes unstable (i.e. oxidizes to CO_2) at $T \geq \sim 570$°C. (B) Carbon saturated fluid ($a_{\text{carbon}} = 1$), $f_{O_2}^{\text{fluid}} = f_{O_2}^{\text{QFM-1}}$. (C) Carbon-undersaturated fluid ($a_{\text{carbon}} = 0.1$), $f_{O_2}^{\text{fluid}} = f_{O_2}^{\text{QFM}}$.

3.2. Fixed atomic H / O ratio

Using X_O as a variable can be illustrated with isobaric–isothermal ternary C–O–H diagrams (Connolly, 1995; Fig. 4). For example, carbon saturated fluids with $X_O = 0.9$ (Fig. 4A) occurs on the intersection of the $X_O = 0.9$ line and the carbon saturation surface (solid square in Fig. 4A), whereas carbon undersaturated fluids occur in the fluid field on the $X_O = 0.9$ line.

Low-temperature fluids (400°C; Fig. 4A) are binary mixtures of either H_2O–CH_4 (low $f_{O_2}^{\text{fluid}}$, $X_O < 1/3$) or H_2O–CO_2 (high $f_{O_2}^{\text{fluid}}$, $X_O > 1/3$). An increase in temperature (at constant X_O) will increase the mole fraction of the carbonic fluid species (Fig. 4A–D) relative to H_2O. At high temperatures, CO and H_2 become significant fluid species in a carbon saturated fluid with X_O approaching 1 or 0, respectively (Fig. 4D). Non-ideal mixing of the fluid species will shift the carbon saturation surface to the H_2O–CO_2 and H_2O–CH_4 joins (Ferry and Baumgartner, 1987; Connolly and Cesare, 1993).

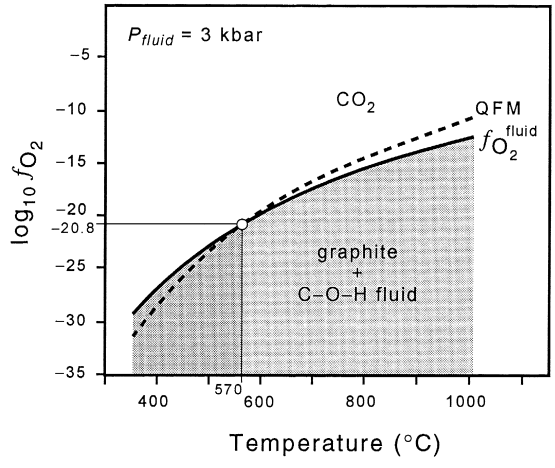

Fig. 2. $f_{O_2}^{\text{QFM}}$ as a function of temperature (dashed line), and the maximum $f_{O_2}^{\text{fluid}}$ for a carbon saturated fluid (solid line) at a fluid pressure of 3 kbar. The shaded area (dark and light) indicates the stability field of graphite. The dark shaded area indicates the stability field of a carbon saturated C–O–H fluid, of which $f_{O_2}^{\text{fluid}} = f_{O_2}^{\text{QFM}}$. The figure shows that the maximum temperature at which a QFM buffered C–O–H fluid can exist in equilibrium with graphite is at ~ 570°C, for which $\log_{10} f_{O_2}^{\text{fluid}} = \log_{10} f_{O_2}^{\text{QFM}} = \sim -20.8$ (see also Fig. 1A).

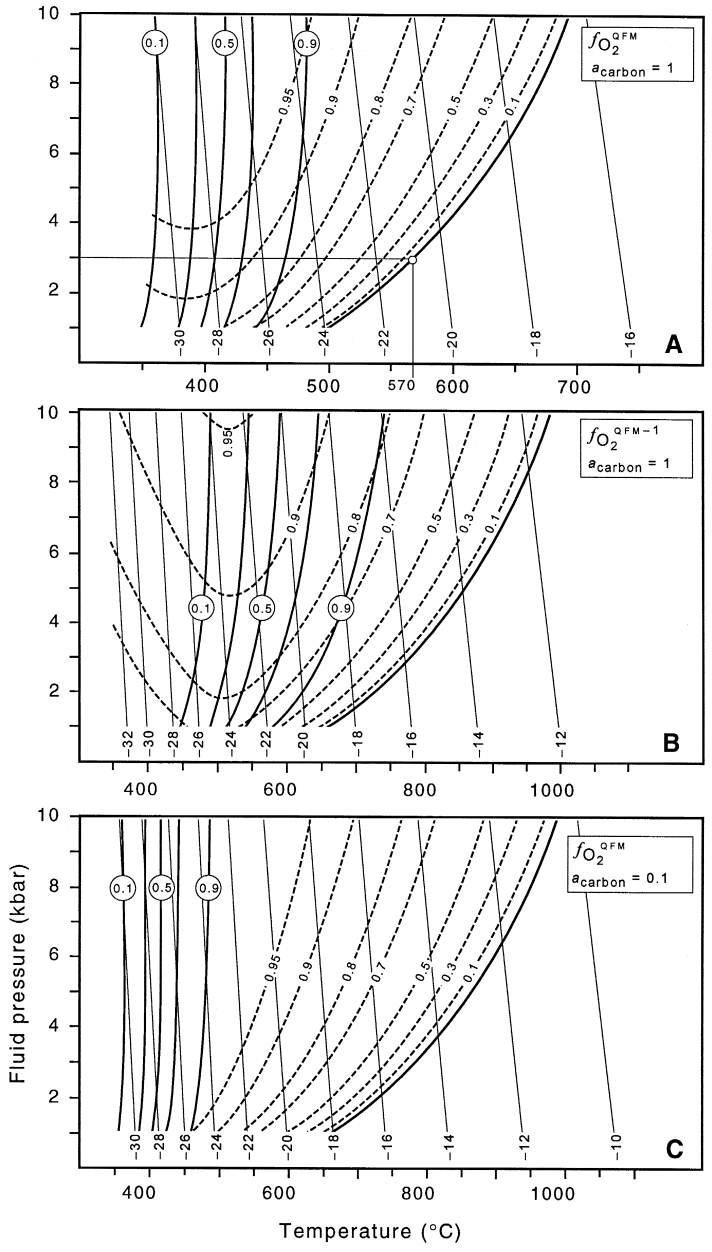

Fig. 3. Pressure–temperature diagrams showing the isopleths for X_{H_2O} (dashed lines), $X_{CO_2}/(X_{CO_2}+X_{CH_4})$ (solid lines, 0.1, 0.3, 0.5, 0.7 and 0.9), and $\log_{10} f_{O_2}^{fluid}$ contours (thin solid lines). The thick solid line indicates the maximum pressure–temperature stability of the C–O–H fluid. (A) $f_{O_2}^{fluid} = f_{O_2}^{QFM}$, $a_{carbon} = 1$. (B) $f_{O_2}^{fluid} = f_{O_2}^{QFM\text{-}1}$, $a_{carbon} = 1$. (C) $f_{O_2}^{fluid} = f_{O_2}^{QFM}$, $a_{carbon} = 0.1$.

For dehydrating graphitic rocks, the metamorphic fluid (H_2O) can only react with graphite, and X_O is, therefore, fixed at a value of 1/3 (H_2O: $n_O = 1$, $n_H = 2$). Fig. 5A shows the isopleths of X_{H_2O} and $\log_{10} f_{O_2}^{fluid}$ contours in a P–T diagram, calculated for a carbon saturated fluid at a constant X_O of 1/3.

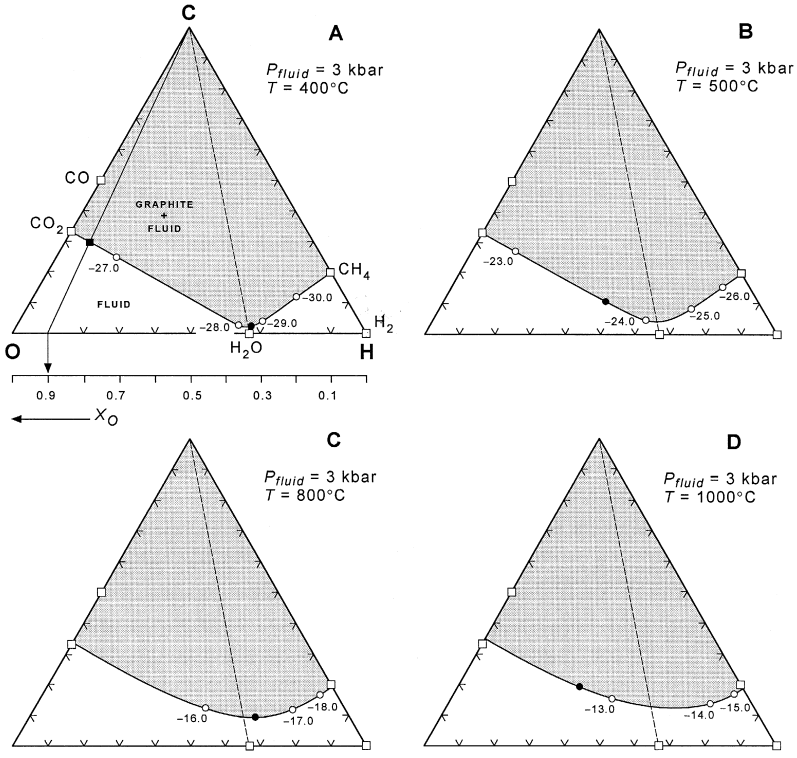

Fig. 4. Ternary C–O–H diagrams at a pressure of 3 kbar and temperatures of (A) 400°C, (B) 500°C, (C) 800°C and (D) 1000°C showing the fluid compositions as a function of X_O. $f_{O_2}^{fluid}$ (open circles) is indicated in $\log_{10}$ intervals for carbon saturated fluids on the carbon saturation surface (solid line). The black circles correspond to $f_{O_2}^{fluid} = f_{O_2}^{QFM}$ (T = 400°C, 500°C), and $f_{O_2}^{fluid} = f_{O_2}^{QFM\text{-}2}$ (T = 800°C, 1000°C). The shaded area represents the fluid + graphite field, the area below the carbon saturation surface are carbon-undersaturated fluids. Fluids with $X_O = 0.9$ (A) occur on the solid line starting from the C apex. The solid square indicates a carbon saturated fluid with $X_O = 0.9$. Carbon saturated fluids with X_O close to 0 are CH_4 ($\pm H_2$)-rich, whereas fluids with X_O close to 1 are CO_2 ($\pm$CO)-rich. The H_2O–C tieline (dashed line) corresponds to fluids with $X_O = 1/3$.

The figure illustrates that dehydration of a graphitic rock should result in H_2O-rich fluids, except for high-T, low-P conditions. In such a fluid, X_{CO_2} and X_{CH_4} are related to each other according to Eq. (18) (Connolly and Cesare, 1993). Substituting Eqs. (19) and (20) into Eq (18) gives:

$$\frac{X_{H_2O} + 2X_{CO_2} + X_{CO} + 2X_{O_2}}{3X_{H_2O} + 2X_{CO_2} + X_{CO} + 2X_{O_2} + 4X_{CH_4} + 2X_{H_2}} = 1/3 \quad (27)$$

which, ignoring X_{O_2}, reduces to:

$$X_{CH_4} + \frac{1}{2}X_{H_2} = X_{CO_2} + \frac{1}{2}X_{CO} \quad (28)$$

Eq. (28) demonstrates that the fluid consists of equal amounts of CO_2 and CH_4, assuming that H_2 and CO occur in negligible amounts (Connolly and Cesare, 1993). Dehydration in graphite poor rocks will lead to almost pure aqueous fluids (Fig. 5B; $a_{carbon} = 0.1$).

4. Application to fluid inclusion studies

Fluid inclusions can provide information on the fluid speciation and density during the P–T evolution of a rock. Analysing the composition of the carbonic fluid phase (including demonstrating the presence of invisible graphite) by means of Raman

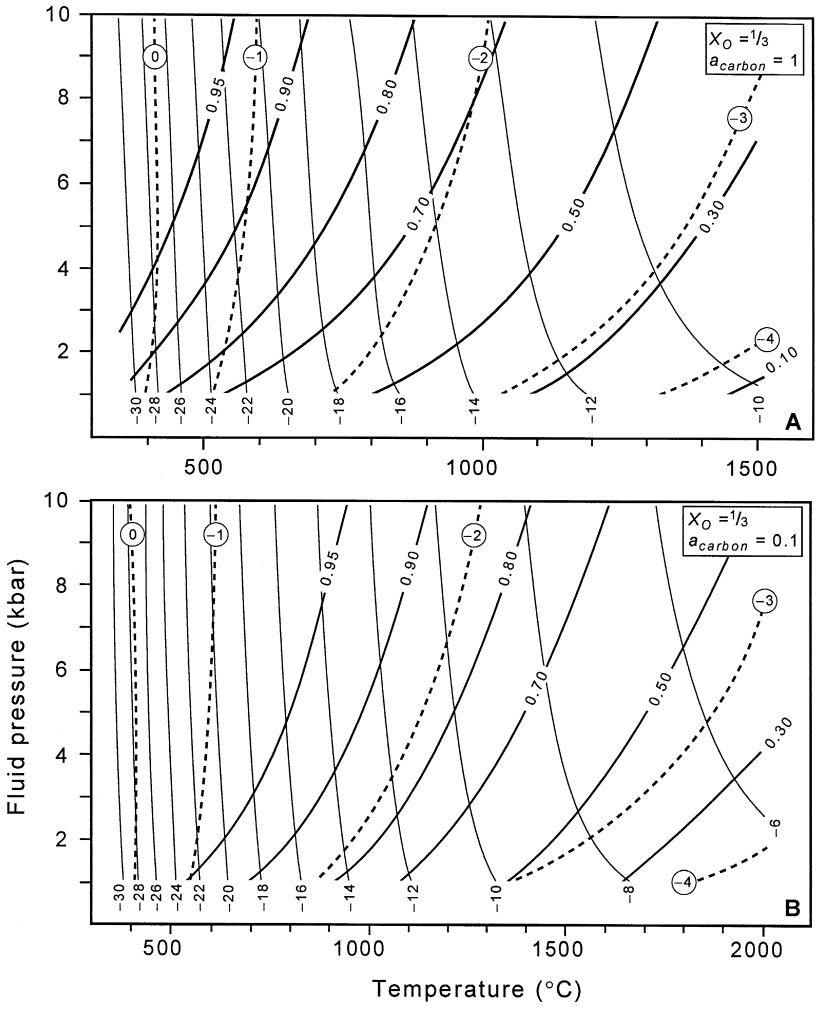

Fig. 5. Pressure–temperature diagrams showing the isopleths for maximum X_{H_2O} (thick solid lines) and $\log_{10} f_{O_2}^{fluid}$ contours (thin solid lines) for a C–O–H fluid, of which X_O is fixed at 1/3. The difference ($\log_{10} f_{O_2}^{fluid} - \log_{10} f_{O_2}^{QFM}$) is indicated with the dashed lines. (A) $a_{carbon} = 1$, (B) $a_{carbon} = 0.1$.

microspectrometry has proven to be a useful and an accurate technique in fluid inclusion studies (e.g., Burke, 1994; Burke, this issue; Burke and Lustenhouwer, 1987). However, an accurate (non-destructive) estimation of X_{H_2O} in fluid inclusions is still a problem (e.g., Boiron and Dubessy, 1994). Therefore, the most reliable compositional variable that can be derived from fluid inclusions is $X_{CO_2}/(X_{CO_2} + X_{CH_4})$. Van den Kerkhof et al. (1991), Frezzotti et al. (1994) and Huizenga and Touret (1999) have demonstrated that $X_{CO_2}/(X_{CO_2} + X_{CH_4})$ values obtained from fluid inclusions can successfully be used to calculate P–T–f_{O_2} trends along which the fluid composition evolved.

Fig. 3 shows that the composition of the carbonic phase, $X_{CO_2}/(X_{CO_2} + X_{CH_4})$, mainly depends on the temperature, assuming that $f_{O_2}^{fluid}$ is buffered by a mineral assemblage. However, the strong influence of $f_{O_2}^{fluid}$ on the position of the $X_{CO_2}/(X_{CO_2} + X_{CH_4})$ isopleths in the P–T diagram makes the carbonic composition not suitable to use as a geothermometer unless $f_{O_2}^{fluid}$ is very well constrained. For example, a

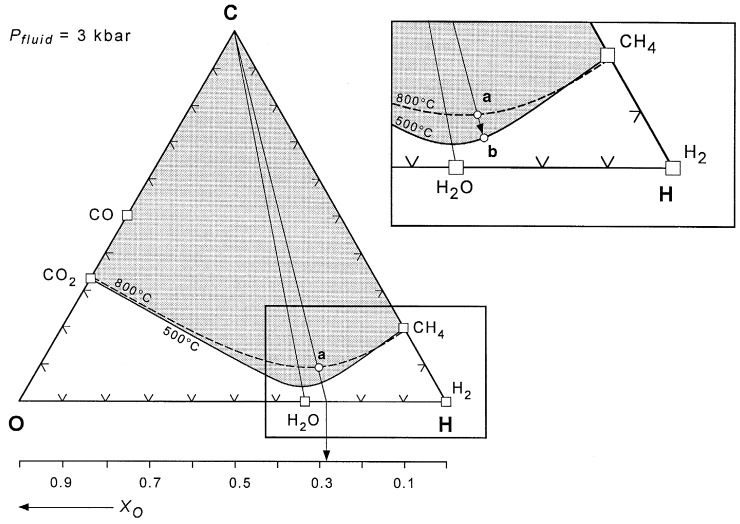

Fig. 6. Isobaric–isothermal C–O–H ternary diagram illustrating graphite precipitation during isobaric cooling (after Cesare, 1995). A carbon-saturated fluid at 800°C and 3 kbar (point **a** in the diagram) with X_O of ~0.3 becomes carbon-saturated during cooling and will precipitate graphite according to reaction (29). The new fluid composition will be located on the 500°C carbon saturation surface (point **b**).

$X_{CO_2}/(X_{CO_2}+X_{CH_4})$ value of 0.5 will give a temperature of ~410°C for $f_{O_2}^{fluid}=f_{O_2}^{QFM}$, and ~470°C for $f_{O_2}^{fluid}=f_{O_2}^{QFM-1/2}$ at a fluid pressure of 3 kbar. Therefore, it is better to use the carbonic fluid com-

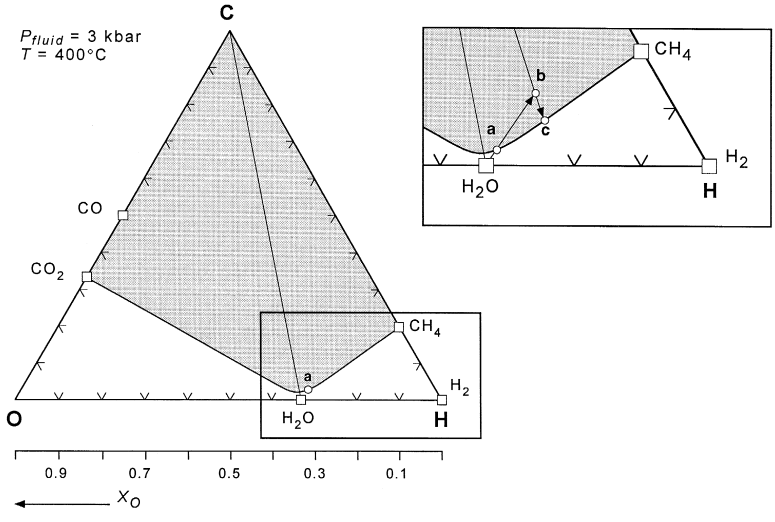

Fig. 7. Isobaric–isothermal C–O–H ternary diagram ($P_{fluid}=3$ kbar, $T=500$°C) demonstrating preferential H_2O leakage and graphite precipitation (after Bakker and Jansen, 1993). Point **a** represents a C–O–H fluid in equilibrium with graphite. H_2O leakage will move the fluid composition towards **b** into the shaded area. As a result, the fluid will re-equilibrate according to reaction (29), i.e. the fluid will move away from the **C** apex (the fluid is depleted in carbon because graphite precipitates), until it reaches the carbon saturation surface (**c**). Initial fluid inclusions with $X_O>1/3$ will show an increase in $X_{CO_2}/(X_{CO_2}+X_{CH_4})$, whereas inclusions with $X_O<1/3$ will show a decrease in $X_{CO_2}/(X_{CO_2}+X_{CH_4})$. $X_{CO_2}/(X_{CO_2}+X_{CH_4})$ remains the same for fluid inclusions with $X_O=1/3$. Changes in molar volume and P_{fluid} during this process are ignored.

position as an indicator of $f_{O_2}^{fluid}$, using independent P–T estimations, rather than using it as an indicator of the temperature at a fixed $f_{O_2}^{fluid}$.

It must be emphasized that C–O–H model calculations in fluid inclusion studies are only valid when the fluid inclusion compositions reflects the composition of the fluid at the time of trapping. It has, however, been pointed out by, e.g., Kreulen (1987), Cesare (1995) and Ridley and Hagemann (1999) that this assumption is certainly not always true and post-entrapment compositional changes in fluid inclusions are probably more the rule than the exception.

4.1. Closed system changes: graphite precipitation

Post-entrapment compositional changes in fluid inclusions behaving as a closed system have been discussed in detail by Dubessy (1984), Kreulen (1987) and Cesare (1995). A fluid inclusion that contains CO_2, and significant amounts of CH_4 ($\pm H_2O$), will re-equilibrate and precipitate graphite during cooling according to the heterogeneous reaction (Fig. 6):

$$CO_2 + CH_4 \rightarrow 2C_{graphite} + 2H_2O \quad (29)$$

where X_O of the fluid does not change (X_O of both reactants and products is $1/3$; Cesare, 1995). It must be emphasized that reaction (29) requires a high activation energy (Ziegenbein and Johannes, 1980), which explains the (metastable) mixtures of CO_2 and CH_4 observed in fluid inclusions at room temperature (Kreulen, 1987; Van den Kerkhof, 1988). If reaction (29) runs to completion, it will either result in graphite-bearing H_2O–CO_2 ($X_{CH_4}^{initial} < X_{CO_2}^{initial}$, i.e. $X_O^{initial} > 1/3$) or in graphite-bearing H_2O–CH_4 fluid inclusions ($X_{CH_4}^{initial} > X_{CO_2}^{initial}$, i.e. $X_O^{initial} < 1/3$).

4.2. Open system changes: selective water leakage

Preferential water from fluid inclusions has been demonstrated experimentally by, e.g., Bakker and Jansen (1990) and can be either strain-induced (Hollister, 1990; Bakker and Jansen, 1994; Cordier et al., 1994) or initiated by a f_{H_2O} gradient, i.e. f_{H_2O} in the fluid inclusion is greater than f_{H_2O} in the intergranular fluid (e.g., Hall and Sterner, 1993; Sterner et al., 1995). Preferential water leakage from a H_2O–CO_2–CH_4 inclusion may trigger reaction (29) (Fig. 7) and if water leakage and reaction (29) occur simultaneously, the fluid inclusion will move along the carbon saturation surface (Bakker and Jansen, 1993). The fluid inclusion may then either become more CO_2 rich ($X_{CH_4}^{initial} < X_{CO_2}^{initial}$, i.e. $X_O^{initial} > 1/3$) or more CH_4-rich ($X_{CH_4}^{initial} > X_{CO_2}^{initial}$, i.e. $X_O^{initial} < 1/3$).

4.3. Open system changes: hydrogen diffusion

Experimental studies (Morgan et al., 1993; Mavrogenes and Bodnar, 1994), and study of fluid inclusions in natural samples (Hall et al., 1991) have shown that fluid inclusions may behave as open systems with respect to hydrogen. The mobility of hydrogen is driven by a difference in f_{H_2} of the intergranular fluid and the fluid inside the inclusion (cf. selective H_2O leakage) and the temperature (Hall and Bodnar, 1990; Hall et al., 1991; Morgan et al., 1993). Experiments by Morgan et al. (1993) carried out at $T = 720°C$ demonstrate that, depending on the fluid density, the following reactions might occur in CO_2 fluid inclusions in quartz when hydrogen moves into the inclusion:

$$CO_2 + 4H_2 \rightarrow CH_4 + 2H_2O \quad (30)$$

This reaction occurs in fluid inclusions with a density lower than ~ 0.75 g cm^{-3}. For high-density fluids, graphite and water will be formed according to the reaction:

$$CO_2 + 2H_2 \rightarrow C_{graphite} + 2H_2O \quad (31)$$

Experiments by Morgan et al. (1993) show that hydrogen diffusion out of an inclusion can trigger the reaction:

$$CH_4 \rightarrow C_{graphite} + 2H_2 \quad (32)$$

and the generated hydrogen will react with CO_2:

$$CO_2 + 2H_2 \rightarrow C_{graphite} + 2H_2O \quad (33)$$

Continuous hydrogen diffusion out of the inclusions may thus either result in graphite-bearing H_2O–CO_2 inclusions ($X_{CH_4}^{initial} < X_{CO_2}^{initail}$ in the initial fluid, i.e. $X_O^{initial} > 1/3$) or in graphite-bearing H_2O inclusions ($X_{CH_4}^{initial} > X_{CO_2}^{initail}$ in the initial fluid, i.e. $X_O^{initial} < 1/3$).

5. Conclusions

CO_2–$CH_4 \pm H_2O$ inclusions without graphite either represent the original fluid present during trapping conditions, or the original fluid inclusion was CO_2-rich ($\pm H_2O$) and has subsequently become enriched in CH_4 due to H_2 diffusion into the inclusion (i.e. reaction (30), for low-density fluids).

Graphite-bearing CO_2–$CH_4 \pm H_2O$ inclusions of which the gas-phase is dominated either by CO_2 or CH_4, are most likely the result of reaction (29), which has not run to completion. This reaction is triggered by (1) cooling, or (2) selective H_2O leakage, or (3) H_2 diffusion out of the inclusion, or by a combination of these factors and will increase the molar volume of the inclusions because of the low molar volume of graphite (5.3 cm^3 mol^{-1}; Holland and Powell, 1998) and, if applicable, the loss of H_2O.

Graphite-bearing H_2O inclusions ($X_O = 1/3$) can be produced by completion of reaction (29) for an inclusion, of which $X_O^{initial} = 1/3$ (Fig. 7). Alternatively, these inclusions can also be formed through continuous hydrogen diffusion out of the inclusion ($X_O^{initial} < 1/3$, reactions (31) and (33)), or continuous hydrogen diffusion into high-density CO_2 fluid inclusions (reactions (31)).

The intensity of post-entrapment changes may be different for inclusions within trails and clusters and depends, amongst others, on the composition and structure of the host mineral (e.g., Morgan et al., 1993; Ridley and Hagemann, 1999). Recognizing these changes requires a detailed study of the inclusions (e.g., Ridley and Hagemann, 1999) and is essential before any model calculations can be done.

Acknowledgements

Acknowledgement is due to the editors of this issue for giving me the opportunity to write this paper. I would like to thank Jacques Touret for his help, inspiration, encouragements, and the discussions on many different aspects of fluid inclusions during the last 10 years. Tom Andersen and Rune Larsen made valuable suggestions to improve the manuscript. This work was financially supported by the Faculty of Earth Sciences, Vrije Universiteit Amsterdam, and the Faculty of Natural Sciences, Rand Afrikaans University.

Appendix A. Explanation of symbols used in the text

Symbol	Explanation
a_{carbon}	Carbon activity
f_i	Fugacity of fluid species i
$f_{O_2}^{fluid}$	f_{O_2} of the fluid phase
$f_{O_2}^{QFM}$	f_{O_2} buffered by the mineral assemblage QFM
$f_{O_2}^{QFM\text{-}1}$	f_{O_2} one $\log_{10}$ unit below $f_{O_2}^{QFM}$
γ_i	fugacity coefficient of species i
$\Delta_r G^O$	Gibbs energy of the reaction
K	Equilibrium constant
n_H	number of moles of hydrogen in the fluid phase
n_O	number of moles of oxygen in the fluid phase
P_{fluid}	fluid pressure
R	gas constant (8.314 J mol^{-1} K^{-1})
T	temperature
V	molar volume
X_i	Mole fraction of species i in a fluid phase
$X_i^{initial}$	Initial mole fraction of species i in a fluid inclusion
X_O	atomic fraction of oxygen relative to oxygen and hydrogen in a fluid phase
$X_O^{initial}$	initial atomic fraction of oxygen relative to oxygen and hydrogen in a fluid inclusion
Z	Compressibility factor ($Z = 1$ for a perfect gas)

References

Anderson, G.M., Crerar, D.A., 1993. Thermodynamics in Geochemistry — The equilibrium model. Oxford Univ. Press, New York.

Aranovich, L.Ya., Newton, R.C., 1996. H_2O activity in concentrated NaCl solutions at high pressures and temperatures measured by the brucite–periclase equilibrium. Contrib. Mineral. Petrol. 125, 200–212.

Bakker, R.J., 1999. Adaption of the Bowers and Helgeson (1983) equation of state to the H_2O–CO_2–CH_4–N_2–NaCl system. Chem. Geol. 154, 225–236.

Bakker, R.J., Jansen, J.B.H., 1990. Preferential water leakage from fluid inclusions by means of mobile dislocations. Nature 345, 58–60.

Bakker, R.J., Jansen, J.B.H., 1993. Calculated fluid evolution path versus fluid inclusion data in the COHN system as exemplified by metamorphic rocks, Rogaland SW Norway. J. Metamorph. Geol. 11, 357–370.

Bakker, R.J., Jansen, J.B.H., 1994. A mechanism for preferential H_2O leakage from fluid inclusions in quartz, base on TEM observations. Contrib. Mineral. Petrol. 116, 7–20.

Belonoshko, A.B., Saxena, S.K., 1991a. A molecular dynamics study of the pressure–volume–temperature properties of supercritical fluids: Part I. H_2O. Geochim. Cosmochim. Acta 55, 381–388.

Belonoshko, A.B., Saxena, S.K., 1991b. A molecular dynamics study of the pressure–volume–temperature properties of supercritical fluids: Part II. CO_2 CH_4, CO, O_2, H_2. Geochim. Cosmochim. Acta 55, 3191–3208.

Belonoshko, A.B., Saxena, S.K., 1992. A unified equation of state for fluids C–O–H–N–S–Ar composition and their mixtures up to very high temperatures and pressures. Geochim. Cosmochim. Acta 56, 3611–3626.

Belonoshko, A.B., Shi, P., Saxena, S.K., 1992. SUPERFLUID: a Fortran-77 program for calculation of Gibbs free energy and volume of C–H–O–N–S–Ar mixtures. Comput. Geosci. 18, 1267–1269.

Boiron, M.-C., Dubessy, J., 1994. Determination of fluid inclusion compositions: microanalytical techniques. In: De Vivo, B., Frezzotti, M.L. (Eds.), Fluid Inclusions in Minerals: Methods and Applications. Virginia Tech, pp. 45–71.

Bowers, T.S., Helgeson, H.C., 1983. Calculation of thermodynamic and geochemical consequences of nonideal mixing in the system H_2O–CO_2–NaCl on phase relations in geological systems: equations of state for H_2O–CO_2–NaCl fluids at high pressures and temperatures. Geochim. Cosmochim. Acta 47, 1247–1275.

Burke, E.A.J., 1994. Raman microspectrometry of fluid inclusions: the daily practice. In: De Vivo, B., Frezzotti, M.L. (Eds.), Fluid Inclusions in Minerals: Methods and Applications. Virginia Tech, pp. 25–44.

Burke, E.A.J., Lustenhouwer, W.J., 1987. The application of a multichannel laser Raman microprobe (Microdil-28®) to the analysis of fluid inclusions. Chem. Geol. 61, 11–17.

Burnham, C.W., Holloway, J.R., Davis, N.F., 1969. Thermodynamic properties of water to 1000°C and 10,000 bars Geol. Soc. America Spec. Paper 132.

Cesare, B., 1995. Graphite precipitation in C–O–H fluid inclusions: closed system compositional and density changes, and thermobarometric implications. Contrib. Mineral. Petrol. 122, 25–33.

Chase, J.M.W., Davies, C.A., Downey, J., Frurip, D.J., McDonald, R.A., Syverud, A.N., 1985. JANAF Thermochemical tables. J. Phys. Chem. Ref. Data 14 (Suppl. 1).

Chatterjee, N.D., 1991. Applied Mineralogical Thermodynamics. Springer-Verlag.

Connolly, J.A.D., 1990. Multivariable phase diagrams: an algorithm based on generalized thermodynamics. Am. J. Sci. 290, 666–718.

Connolly, J.A.D., 1995. Phase diagram methods for graphitic rocks and application to the system C–O–H–FeO–TiO_2–SiO_2. Contrib. Mineral. Petrol. 119, 94–116.

Connolly, J.A.D., Cesare, B., 1993. C–O–H–S fluid compositions and oxygen fugacity in graphitic metapelites. J. Metamorph. Geol. 11, 379–388.

Cordier, P., Doukhan, J.C., Ramboz, C., 1994. Influence of dislocations on water leakage from fluid inclusions in quartz: a quantitative reappraisal. Eur. J. Mineral. 6, 745–752.

Dubessy, J., 1984. Simulation des équilibres chimiques dans le système C–O–H. Conséquences méthodologiques pour les inclusions fluides. Bull. Mineral. 107, 155–168.

Eugster, H.P., Skippen, G.B., 1967. Igneous and metamorphic reactions involving gas equilibria. In: Abelson, P.H. (Ed.), Researches in Geochemistry, vol. 2, pp. 492–520.

Ferry, J.M., Baumgartner, L., 1987. Thermodynamic models of molecular fluids at the elevated pressures and temperatures of crustal metamorphism. In: Carmichael, I.S.E., Eugster, H.P. (Eds.), Thermodynamic Modeling of Geological Materials: Minerals, Fluids, and Melts. Min. Soc. Am. Rev. Min., vol. 17, pp. 323–365.

Flowers, G.C., Helgeson, H.C., 1983. Equilibrium and mass transfer during progressive metamorphism of siliceous dolomites. Am. J. Sci. 283, 230–286.

French, B.M., 1966. Some geological implications of equilibrium between graphite and a C–O–H gas at high temperatures and pressures. Rev. Geophys. 4, 223–253.

Frezzotti, M.L., Di Vincenzo, G., Ghezzo, C., Burke, E.A.J., 1994. Evidence of magmatic CO_2-rich fluids in peraluminous graphite-bearing leucogranites from Deep Freeze Range. Contrib. Mineral. Petrol. 117, 111–123.

Frost, B.R., 1979. Mineral equilibria involving mixed-volatiles in a C–O–H fluid phase: the stabilities of graphite and siderite. Am. J. Sci. 279, 1033–1059.

Glassley, W., 1982. Fluid evolution and graphite genesis in the deep continental crust. Nature 295, 229–231.

Hall, D.L., Bodnar, R.J., 1990. Methane in fluid inclusions from granulites: a product of hydrogen diffusion? Geochim. Cosmochim. Acta 54, 641–651.

Hall, D.L., Sterner, M.S., 1993. Preferential water loss from synthetic fluid inclusions. Contrib. Mineral. Petrol. 114, 489–500.

Hall, D.L., Bodnar, R.J., Craig, J.R., 1991. Evidence for postentrapment diffusion of hydrogen into peak metamorphic fluid inclusions from the massive sulfide deposit at Ducktown, Tennesee. Am. Mineral. 76, 1344–1355.

Holland, H.D., 1965. Some applications of thermochemical data to problems of ore deposits: Part II. Mineral assemblages and the compositions of ore-forming fluids. Econ. Geol. 60, 1101–1166.

Holland, T.J.B., Powell, R., 1998. An internally consistent thermodynamic data set for phases of petrological interest. J. Metamorph. Geol. 16, 309–343.

Hollister, L.S., 1990. Enrichment of CO_2 in fluid inclusions in quartz by removal of H_2O during crystal–plastic deformation. J. Struct. Geol. 12, 895–901.

Holloway, J.R., 1977. Fugacity and activity of molecular species in supercritical fluids. In: Fraser, D. (Ed.), Thermodynamics in Geology. Reidel, Boston, pp. 161–181.

Holloway, J.R., 1981. Compositions and volumes of supercritical fluids in the Earth's crust. In: Hollister, L.S., Crawford, M.L. (Eds.), Short Course in Fluid Inclusions: Applications to Petrology. MAC Short Course Handbook, vol. 6, pp. 13–36.

Holloway, J.R., 1984. Graphite–CH_4–H_2O–CO_2 equilibria at low-grade metamorphic conditions. Geology 12, 455–458.

Holloway, J.R., 1987. Igneous fluids. In: Carmichael, I.S.E., Eugster, H.P. (Eds.), Thermodynamic Modeling of Geological Materials: Minerals, Fluids, and Melts. Min. Soc. Am. Rev. Min., vol. 17, pp. 211–233.

Huebner, J.S., 1971. Buffering techniques for hydrostatic systems at elevated pressures. In: Ulmer, G.C. (Ed.), Research Techniques for High Pressure and High Temperature. Springer-Verlag, New York, pp. 123–177.

Huizenga, J.M., Touret, J.L.R., 1999. Fluid inclusions in shear zones: the case of the Umwindsi shear zone in the Harare–Shamva–Bindura greenstone belt, NE Zimbabwe. Eur. J. Mineral. 11, 1079–1090.

Jacobs, K.G., Kerrick, D.M., 1981. Methane: an equation of state with application to the ternary system H_2O–CO_2–CH_4. Geochim. Cosmochim. Acta 45, 607–614.

Kreulen, R., 1987. Thermodynamic calculations in the C–O–H system applied to fluid inclusions: are fluid inclusions unbiassed samples of ancient fluids? Chem. Geol. 61, 59–64.

Labotka, T.C., 1991. Chemical and physical properties of fluids. In: Kerrick, D. (Ed.), Contact Metamorphism. Mineral. Soc. Am. Rev. Mineral., vol. 26, pp. 43–104.

Lamb, W.M., Valley, J.W., 1985. C–O–H fluid calculations and granulite genesis. In: Tobi, A.C., Touret, J.L.R. (Eds.), The Deep Proterozoic Crust in the North Atlantic Provinces. NATO ASI Series C, vol. 158, pp. 119–131.

Larsen, R.B., 1993. GEOFLUID: a Fortran 77 program to compute chemical properties of gas species in C–O–H fluids. Comput. Geosci. 19, 1295–1320.

Mavrogenes, J.A., Bodnar, R.J., 1994. Hydrogen movement into and out of fluid inclusions in quartz: experimental evidence and geological implications. Geochim. Cosmochim. Acta 58, 141–148.

Miyashiro, A., 1994. Metamorphic Petrology. UCL press.

Morgan, G.B., I-Ming, C., Pateris, C., Olsen, S.N., 1993. Re-equilibration of CO_2 fluid inclusions at controlled hydrogen fugacities. J. Metamorph. Geol. 11, 155–164.

Ohmoto, H., Kerrick, D., 1977. Devolatilization equilibria in graphitic systems. Am. J. Sci. 277, 1013–1044.

Ramboz, C., Schnapper, D., Dubessy, J., 1985. The $P-\overline{V}-T-X-f_{O_2}$ evolution of H_2O–CO_2–CH_4-bearing fluid in a wolframite vein: reconstruction from fluid inclusion studies. Geochim. Cosmochim. Acta 49, 205–219.

Redlich, O., Kwong, J.N.S., 1949. On the thermodynamics of solutions. V. Chem. Rev. 44, 233–244.

Rhyzhenko, B.N., Volkov, V.P., 1971. Fugacity coefficients of some gases in a broad range of temperatures and pressures. Geochim. Intern. 8, 468–481.

Ridley, J., Hagemann, S.G., 1999. Interpretation of post-entrapment fluid-inclusion re-equilibration at the Three Mile Hill, Marvel Loch and Griffins Find high-temperature lode gold deposits, Yilgarn Craton, Western Australia. Chem. Geol. 154, 257–278.

Saul, A., Wagner, W., 1989. A fundamental equation of water covering the range from the melting line to 1273 K at pressures up to 25,000 MPa. J. Phys. Chem. Ref. Data 18, 370–375.

Saxena, S.K., Fei, Y., 1987a. High pressure and high temperature fugacities. Geochim. Cosmochim. Acta 51, 783–791.

Saxena, S.K., Fei, Y., 1987b. Fluids at crustal pressures and temperatures: Part I. Pure species. Contrib. Mineral. Petrol. 95, 370–375.

Shaw, H.R., Wones, D.R., 1964. Fugacity coefficients for hydrogen gas between 0° and 1000°C, for pressures to 3000 atm. Am. J. Sci. 262, 918–929.

Shi, P., Saxena, S.K., 1992. Thermodynamic modelling of the C–O–H–S fluid system. Am. Mineral. 77, 1038–1049.

Skippen, G.B., Marshall, D.D., 1991. The metamorphism of granulites and devolatilization of the lithosphere. Can. Mineral. 29, 693–705.

Spear, F.S., 1993. Metamorphic phase equilibria and pressure–temperature–time paths. Mineral. Soc. Am. Monogr.

Sterner, S.M., Bodnar, R.J., 1991. Synthetic fluid inclusions. X: Experimental determination of $P-V-T-X$ properties in the CO_2–H_2O system to 6 kbar and 700°C. Am. J. Sci. 291, 1–54.

Sterner, S.M., Hall, D.L., Keppler, H., 1995. Compositional re-equilibration of fluid inclusions in quartz. Contrib. Mineral. Petrol. 119, 1–15.

Van den Kerkhof, A.M., 1988. The system CO_2–CH_4–N_2 in fluid inclusions: theoretical modelling and geological applications. PhD Thesis, Free Univ. Amsterdam, The Netherlands.

Van den Kerkhof, A.M., Touret, J.L.R., Maijer, C., Jansen, J.B.H., 1991. Retrograde methane dominated fluid inclusions from high-temperature granulites of Rogaland, SW Norway. Geochim. Cosmochim. Acta 55, 2533–2544.

Wopenka, B., Pasteris, J.D., 1993. Structural characterization of kerogens to granulite-facies graphite: applicability of Raman microprobe spectroscopy. Am. Mineral. 78, 533–557.

Ziegenbein, D., Johannes, W., 1980. Graphite in C–O–H fluids: an unsuitable compound to buffer fluid composition at temperatures up to 700°C. N. Jb. Mineral. Mh. 7, 289–305.